*The Nucleus* ***52****, No. 4 (2015) 204-208*

*www.thenucleuspak.org.pk*

**The Nucleus**

**ISSN 0029-5698 (Print)**

**ISSN 2306-6539 (Online)**

# Dielectric Characterization of $XAl_2O_4$ (X = Mg, Zn, Ni) Spinel Ceramics

M. Azam, S. Atiq, G. M. Mustafa*, S. Riaz and S. Naseem

*Centre of Excellence in Solid State Physics, University of the Punjab, Quaid-e-Azam Campus, Lahore, Pakistan*

*azamali796@gmail.com;satiq.cssp@pu.edu.pk; gmmustafa25@gmail.com; saira_cssp@yahoo.com; shahzad_naseem@yahoo.com*

ARTICLE INFO

*Article history* :
*Received : 01 September, 2015*
*Revised : 30 October, 2015*
*Accepted : 18 December,2015*

*Keywords* :
*Spinel Ceramics,*
*Sol-gel,*
*Impedance Analysis,*
*Morphology*

ABSTRACT

*Spherical nanoparticles of $XAl_2O_4$ (X = Mg, Zn, Ni) ceramics with large surface area and finely distributed grains, were successfully synthesized by sol-gel auto-combustion method. The formation of spinel structure of $XAl_2O_4$ nanoparticles was confirmed by X-ray diffraction. Dielectric tangent loss was decreased as the frequency was increased while a slight increase in the dielectric parameters was observed as the temperature was increased, mainly due to the thermally activated charge carriers. The behavior of real and imaginary parts of impedance has also been discussed which confirms the results from the tangent loss plot. Energy dispersive X-ray spectroscopy gives the true stoichiometric at% and wt% contents of various elements present in the samples. The grain size of the synthesized sample range from 20-70 nm and were obtained when the samples were sintered at 900 ºC for 4 hrs.*

## 1. Introduction

Ceramics having general formula $AB_2O_4$ possess spinel structure with space group Fd3m, A and B being divalent and trivalent cations, respectively. In normal spinel structure, divalent cations occupy 8 tetrahedral interstices and trivalent cations occupy 16 octahedral interstices. In case of inverse spinel structure, the general formula becomes $(B)[AB]_2O_4$, where 8 divalent together with 8 trivalent cations occupy 16 octahedral interstices and 8 trivalent cations occupy 8 tetrahedral sites [1-3].

Among a long list of ceramics, nanocrystalline material of the form $XAl_2O_4$ (X = Mg, Zn, Al) is among a very attractive class of materials, with appealing characteristics such as high melting point (2135 ºC), excellent mechanical strength at elevated temperature, low dielectric constant, good catalytic property, excellent thermal shock resistance and transparency from the near-UV (ultraviolet) to the mid-IR (infra-red) range [4, 5]. Owing to these excellent properties, these materials are very widely used in different industries, e.g. as refractory materials [6], humidity sensors [7], transparent ceramics [8], in metallurgical, electrochemical and chemical fields [9, 10]. In electric and electronic devices, dielectric materials are very widely used in different components.

Few attempts have already been reported to synthesize $XAl_2O_4$ spinel compounds using various chemical methods including spray drying techniques or plasma spray decomposition of oxides [11], combustion of metal nitrates and urea synthesis [12], self-heat-sustained (SHS) technique [13], sonochemical method [14], hydrothermal method [15] and sol–gel citrate technique [16]. In the present study, sol-gel auto-combustion method has been utilized which has emerged as an excellent technique to prepare spinel nanoparticles in phase pure form. This route is very cost effective, energy efficient and time saving for the preparation of oxide nanoparticles. Using this method, materials with specific surface areas up to 250 $m^2g^{-1}$ have been obtained by calcining the precursors.

The purpose of present study is to investigate the structural correlation among three spinel ceramics of the form $XAl_2O_4$ (X = Mg, Zn, Al) and the consequent effects on the dielectric, compositional and morphological characteristics of these ceramic samples, which have been synthesized by a low cost sol-gel auto combustion method.

## 2. Experimental

In order to prepare $XAl_2O_4$ (Mg, Zn, Al) samples, stoichiometric amounts of starting materials such as aluminum nitrate $Al(NO_3)_3.9H_2O$ (98.5 %, MERCK, 3.55 g), zinc nitrate $Zn(NO_3)_2.6H_2O$ (PANREAC, 98 %, 1.42 g) and urea $CH_4N_2O$ (99.5 %, MERCK, 3.0 g) were dissolved in deionized water separately and then mixed together to make a homogeneous and transparent 50 mL solution. The solution (kept in a beaker) was magnetically stirred at 90 ºC for about 1 hr to get a thick and transparent gel. When the gel was formed, the magnetic stirring was stopped and the temperature was increased to 300 ºC, gradually. After a while, the gel was burnt as a result of self-ignited combustion reaction. The end product was a dark and brownish powder. The powder

* Corresponding author

was ground by an Agate mortar and pestle in order to homogenize the particle size. The obtained powder samples were sintered at 950 ºC for 4 hrs, by using Nabertherm GmbH (SN 271488) furnace, in order to improve the crystal structure of the ceramic samples. The crystal structure was determined using a Bruker D/8 Advance X-ray Diffractometer (XRD). Morphology and chemical stoichiometry has been discussed using a scanning electron microscopy with an attached accessory for energy dispersive X-ray spectroscopy. A Wayne Kerr (6500B) impedance spectroscopy has been utilized to investigate the frequency and temperature dependent dielectric characteristics of the samples. For the dielectric measurements, the powder samples were pelletized having a diameter of 10 mm, using an Apex hydraulic press. A pressure of 3.5 ton was applied for two min in each case.

## 3. Results and Discussion

### *3.1 Structural Analysis*

The pattern, positions and the intensities of the peaks in a diffraction pattern provide information about the crystal structure, unit cell and the atomic positions, respectively. Fig. 1 shows the XRD patterns of $XAl_2O_4$ (Mg, Zn & Ni) samples. High intensity diffraction peaks were observed at 2θ values of 31.3º, 36.9º, 44.9º, 55.9º, 59.5º, 65.4º, 68.9º, 74.3º and 77.4º, well matched with previously reported results [2, 4, 15]. The indexing of these diffraction peaks was performed by following the procedure as laid down by B. D. Cullity [17]. Very small impurity peaks belonging to ZnO were recognized as indicated by ♦ [JCPD # 00-005-0664]. All the three

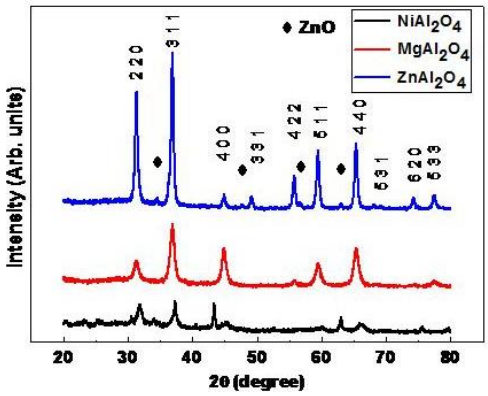


Fig. 1: Comparison of XRD pattern of samples $XAl_2O_4$ (X = Mg, Zn, Ni). It can be seen that the three samples has same crystal structure

patterns revealed the cubic spinel structure, a characteristic structure of spinel, $MgAl_2O_4$. The indexing was well-matched with the JCPDS # 01-084-0377 for $MgAl_2O_4$, 01-073-1961 for $ZnAl_2O_4$ and 00-010-0339 for $NiAl_2O_4$. Hence, the formation of pure crystalline phase of $XAl_2O_4$ spinel structure with space group Fd-3m was confirmed. The lattice constant of $XAl_2O_4$ (Mg, Zn & Ni) has been calculated by the following Eq. 1.

$$a = \frac{\lambda}{2Sin\theta}\sqrt{h^2 + k^2 + l^2} \quad (1)$$

The calculated lattice constant for cubic symmetry 8.0652 Å, 8.0916 Å and 8.0608 Å were in good agreement with the reported values in the respective JCPDS files.

### *3.2. Frequency Dependent Tangent Loss*

Fig. 2 shows a comparison of tangent loss as a function of frequency for three samples $XAl_2O_4$ (X = Mg, Zn & Ni) in the range of 1 kHz to 10 MHz. It is clear that as the applied frequency is increased, the value of tangent loss is decreased. In the frequency range of $10^3$ - $10^4$ Hz, the values of all the samples decreased linearly but in the MHz region, the behavior of $MgAl_2O_4$ was different compared to the other two samples. The resonance seen in the plot of $MgAl_2O_4$ might be attributed to the polarization relaxation phenomenon occurring at this particular frequency region [18]. The polarization in ceramic materials can be explained by the Maxwell-Wagner interfacial polarization phenomenon [19]. According to this model, the dielectric material is composed of double layers; one is highly conducting grains and 2nd is insulating grain boundaries. The value of tanδ approaches to maximum value at a certain frequency. This behavior may be due to the resonance between applied frequency and polaron hopping frequencies. At lowest frequency, the value of tanδ is high because more energy is required for polarization in the grain boundaries but at high frequency, polarization is inhibited due to grains, due to which at high frequency, the value of tanδ becomes lowest.

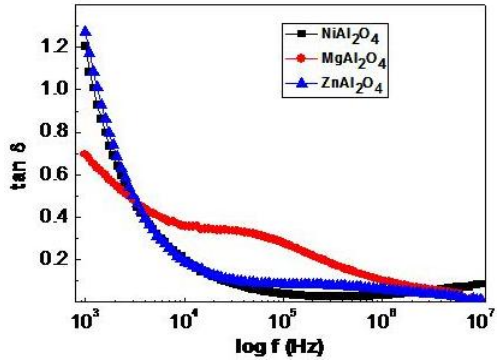


Fig. 2: Loss tangent factor of $XAl_2O_4$ (X = Mg, Zn, Ni) as a function of frequency

### *3.3 Temperature Dependent Tangent Loss*

The variation in tanδ as a function of temperature for $XAl_2O_4$ samples at three different frequencies, 1.6 kHz, 20 kHz and 1 MHz is shown in Fig. 3. It is observed that the value of loss factor increased slightly for all frequency ranges, a characteristic behavior attributed to the

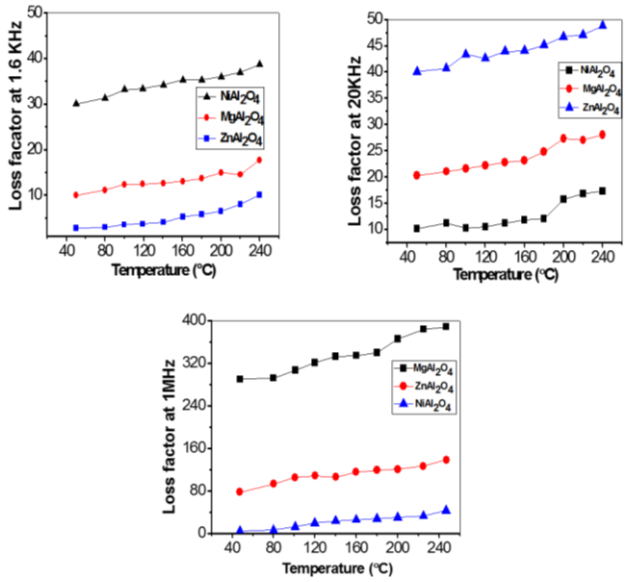


Fig. 3: Value of loss tangent of three samples $XAl_2O_4$ as a function of temperature at frequency (a) 1.6 kHz, (b) 20 kHz, and (c)1MHz

insulating nature of the synthesized samples. The increase in value of loss factor with increase in temperature is due to the thermally activated charge carriers and increased electron exchange interaction. This fact may be due to dipolar and interfacial polarization which depends upon the temperature. Therefore, when the temperature is increased, the AC electrical conductivity increases which enhances the electric polarization which in turn, increases the value of loss factor. It may be considered that the prepared sample based on the inhomogeneous nature of the dielectric structure corresponding to the two layers model in which the grain boundaries are effective at lower frequency and grains at higher frequency.

### *3.4 Variation in Impedance as a Function of Frequency*

The variation in real and imaginary part of impedance as a function of frequency is shown in Fig. 4. It is clear that both the real and imaginary parts of impedance decrease with increasing the frequency which represents

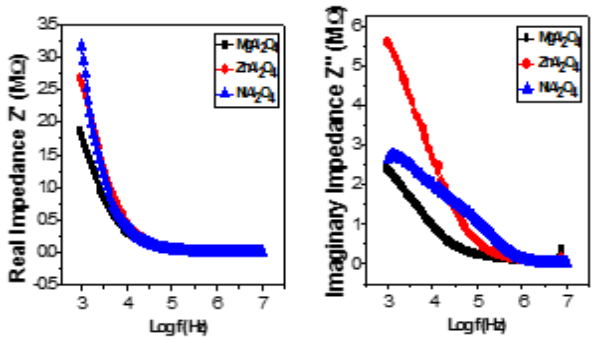


Fig. 4: (a) Comparison of real part of Impedance of $XAl_2O_4$,
(b) Comparison of imaginary part of Impedance of $XAl_2O_4$

the possibility of enhancing the AC conductivity. It has been reported that in ceramic materials, larger space charge polarization appears at lower frequency [20], well in agreement with the present study. The merging of all the curves of real part (Z′) as well as imaginary part (Z″) of impedance in the high frequency region suggests a possible release of space charge and a consequent lowering of the barrier properties in the materials.

Fig. 5 shows the Nyquist plots for the three samples obtained at room temperature in the frequency range from 1 kHz to 10 MHz. Three types of semicircles are usually observed in the Nyquist plots, each belonging to three different electrically active regions. First semicircle, attributed to the surface effects, appears at very low frequency. Second, appearing at intermediate frequencies is related to the grain boundaries. Last one, concerned with the electrical effects within the grains, appears at very high frequencies. In our case, measurements were obtained at room temperature and in the intermediate frequency range so the obtained pattern is nearly semi-circular (showing only a part of second semicircle) having their centres lying off the real (Z′) axis which was indicative of non-Debye type relaxation with a distribution of relaxation times instead of a single relaxation process. In general, the relaxation time for grain boundary region is much larger than that for the grains and therefore its response relaxes at lower frequencies. Thus the arcs obtained in the Nyquist plot correspond to the grain boundary effects.

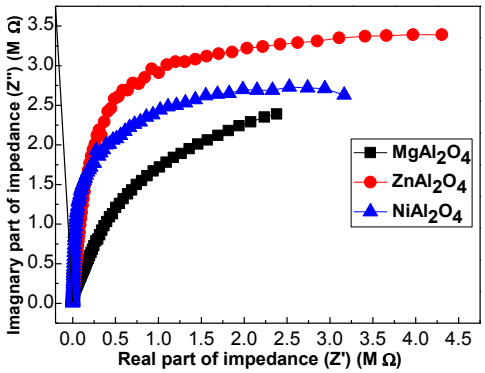


Fig. 5: Imaginary part of impedance (Z″) vs Real part of impedance (Z′)

### *3.5 EDX Analysis of $XAl_2O_4$*

Fig. 6 shows that energy dispersive X- rays Spectroscopy (EDX) of prepared material. No impurity peaks were detected in the spectra of three samples. The spectra show the presence of Mg, Zn, Ni, Al and O in the desired stoichiometric ratio in $XAl_2O_4$ ceramic samples. The evaluated *at*% and *wt*% of all the elements have been provided in Table 1.

Table 1: *at* % and *wt* % of different elements in three samples

| Sample | Mg | | Zn | | Ni | | Al | | O | |
|---|---|---|---|---|---|---|---|---|---|---|
| | *wt%* | *at%* | *wt%* | *at%* | *wt%* | *at%* | *wt%* | *at%* | *wt%* | *at%* |
| $MgAl_2O_4$ | 17.89 | 15.07 | - | - | - | - | 38.68 | 29.36 | 43.43 | 55.58 |
| $ZnAl_2O_4$ | - | - | 25.96 | 9.65 | - | - | 35.79 | 32.24 | 38.25 | 58.11 |
| $NiAl_2O_4$ | - | - | - | - | 45.77 | 23.08 | 31.10 | 34.12 | 23.13 | 42.80 |

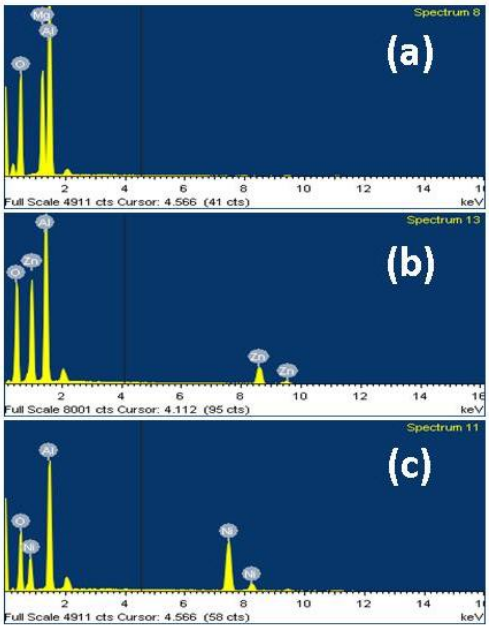


Fig. 6: EDX spectra of (a) $MgAl_2O_4$, (b) $ZnAl_2O_4$ and (c) $NiAl_2O_4$ nanoparticles

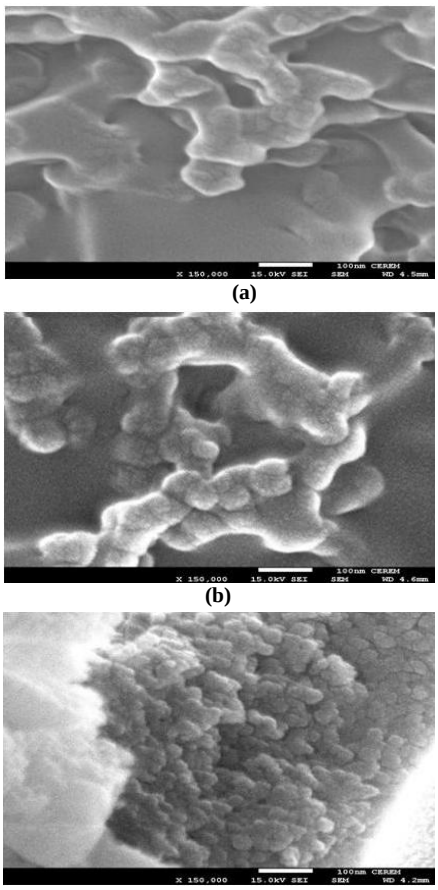


Fig. 7: SEM micrographs of (a) $MgAl_2O_4$, (b) $ZnAl_2O_4$ and (c) $NiAl_2O_4$ nanoparticles

### *3.6 Structural Morphology*

The SEM micrographs of $XAl_2O_4$ materials sintered at 900 ºC for 4 hrs are shown in the Fig. 7. the grain size is found to range between 20-70 nm, using line intercept method. Previously Wei et al. prepared nanosized zinc aluminate spinel by the thermal decomposition of Zn–Al gel prepared by sol–gel technique using oxalic acid as a chelating agent [21]. The sample obtained by heating the precursor at 700 °C for 5 hrs were single-phase cubic materials, having the spinel-type structure. The particle size of 15–20 nm was measured by transmission electron microscopy (TEM).

## 4. Conclusion

A series of ceramic samples with a general formula of $XAl_2O_4$ (X = Mg, Zn, Ni) have been synthesized using sol-gel auto-combustion technique. Indexing of the diffraction peaks obtained using X-ray diffraction was performed by following a complete procedure as described by Cullity. Lattice parameters were of the samples were found in accordance with standard data of these spinel compounds. The values of dielectric parameters were high at low frequency which decreased as the frequency was increased attributed to the reason as described by Maxwell-Wagner interfacial polarization phenomenon. The dielectric parameters showed a slight increasing trend as the temperature was increased to 240 ºC, which could be due to the thermally induced conduction mechanism. The real and imaginary parts of impedance as a function of frequency have also been discussed in detail. EDX analysis confirmed that elements present in the samples were in required stoichiometric ratios. Surface morphology of the samples exhibited spherical shaped grains with well separated grain boundaries having a grain size in the range of 20-70 nm.

## References

[1] K.E. Sickafus and J.M. Wills, "Structure of Spinel", J. Am. Ceram. Soc., vol. 82, pp. 3279-3292, December 1999.

[2] K. Mocala and A. Navrotsky, "Structural and Thermodynamic Variation in Nickel Aluminate Spinel", J. Am. Ceram. Soc., vol. 72, pp. 826-832, May 1989.

[3] J.N. Roelofsen, R.C. Peterson and M. Raudsepp, "Structural variation in nickel aluminate spinel ($NiAl_2O_4$)", Am. Mineral., vol. 77, pp. 522-528, 1992.

[4] I. Ganesh, "A review on magnesium aluminate ($MgAl_2O_4$) spinel: Synthesis, processing and applications", Inter. Mater. Rev., vol. 58, pp. 63-112, 2013.

[5] J. T. Bailey and R. Russell, "Sintered spinel ceramics", Am. Ceram. Soc. Bull., vol. 47, pp. 1025-1029, 1968.

[6] M. A. Sainz and A. Caballero, "Aluminum oxycarbide formation on carbon-coated $Al_2O_3$_MgO spinel", Key Engineering Materials, vol. 132-136, pp. 864-847, 1997.

[7] J.G. Li, T. Ikegami and T. Mori, "Fabrication of translucent magnesium aluminum spinel ceramics", J. Am. Ceram. Soc., vol. 85, pp. 2866–2868, November 2000.

[8] G. Gusmano, G. Montesperelli and G. Mattogno, "Microstructure and electrical properties of $MgAl_2O_4$ thin films for humidity sensing", J. Am. Ceram. Soc., vol. 76, pp. 743-750, March 1993.

[9] R. Smith, D. Bacorisen and K. E. Sickafus, "Dynamical simulations of radiation damage in magnesium aluminate spinel, $MgAl_2O_4$", J. Phys. Condens. Matter, vol. 17, pp. 875-891, 2005.

[10] G. Baudin, R. Martinez and P. Pena, "High-temperature mechanical behaviour of stoichiometric magnesium spinel", J. Am. Ceram. Soc., vol. 78, pp. 1857-1862, July 1995.

[11] V. Montouillout and J. P. Coutures, "Characterization of $MgAl_2O_4$ Precursor powders prepared by aqueous route", J. Am. Ceram. Soc., vol. 82, pp. 3299-3304, December 1999.

[12] S. Bhaduri., S.B. Bhaduri and K.A. Prisbrey, "Auto ignition synthesis of nanocrystalline $MgAl_2O_4$ and related nanocomposites", J. Mater. Res., vol. 14, pp. 3571-3580, 1999.

[13] L. R. Ping, A. M. Azad and T. W. Dung, "Magnesium aluminate ($MgAl_2O_4$) spinel produced via self-heat-sustained (SHS) technique", Mater. Res. Bull., vol. 36, pp. 1417-1430, 2001.

[14] P. Jeevanandam, Y. Koltypin and A. Gedanken, "Preparation of nanosized nickel aluminate spinel by a sonochemical method", Mater. Sci. Engg., vol. 90, pp. 125-132, March 2002.

[15] M. Zawadzki, "Hydrothermal synthesis of nanoporous zinc aluminate with high surface area", Mater. Res. Bull., vol. 35, pp. 109-114, 2000.

[16] A. Saberi, F. G. Fard, M. W. Porada and Z. Negahdari, "A novel approach to synthesis of nanosize $MgAl_2O_4$ spinel powder through sol–gel citrate technique and subsequent heat treatment", Ceram. Inter., vol. 35, pp. 933-937, April 2009.

[17] B. D. Cullity and S. R. Stock, "Elements of X-ray diffraction", 3rd edition, 2001, Prentice Hall, New Jersey, USA.

[18] Y. Han, L. Li, W. Xia, Y. Liu and X. Ren, "Dielectric relaxation in $LiNbO_3$-$MgAl_2O_4$ nanocomposite", Mater. Lett., vol. 83, pp. 94-96, 2012.

[19] S. Angappan, L. J. Berchmans and C.O. Augustin, "Sintering behavior of $MgAl_2O_4$ – a prospective anode material", Mater. Lett., vol. 58, pp. 2283-2289, 2004.

[20] M. J. Iqbal, B. Ismail, C. Rentenberger and H. Ipser, "Modification of physical properties of semiconducting $MgAl_2O_4$ by doping with a binary mixture Co and Zn ions", Mater. Res. Bull., vol. 46, pp. 2271-2277, 2011.

[21] B.X. Weiand and D.Chen, "Synthesis and characterization of nano sized zinc aluminate spinel by sol-gel technique", Mater. Lett., vol. 60, pp. 823-827, March 2006.